SUPRA-CANONICAL INITIAL $^{26}Al/^{27}Al$ FROM A REPROCESSED ALLENDE CAI. A. G. Kerekgyarto[1], C. R. Jeffcoat[1], T. J. Lapen[1], R. Andreasen[1], M. Righter[1], D. K. Ross[2,3], J. I. Simon[3], [1]Department of Earth and Atmospheric Sciences, University of Houston, Houston, Tx 77204 (agkerekgyarto@uh.edu), [2]Jacobs Tech, NASA-JSC, Houston, Tx 77058. [3]Center for Isotope Cosmochemistry and Geochronology, ARES NASA-JSC, Houston, Tx 77058.

Introduction: Calcium-, aluminum-rich inclusions (CAIs) are part of the first crystalline solids to form in our Solar System and as such, they are used to represent its origins [1]. EK 459-5-1 is a course grained, type B1 CAI from the Allende meteorite. It is comprised of a spinel-fassaite-anorthite-melilite bearing core and ~2mm mantle of mostly melilite. The inner most, core-ward section of the mantle shows an oscillatory zoning of major elements, corresponding to the solid solution series of melilite (Fig. 1, *top*). Type B CAIs, also referred to as igneous, are thought to have crystallized at least in part from a melt of prior condensate materials, dust and/or even prior CAIs [2, 3]. The formation mechanism of the B1 mantle is still unknown. It has been proposed to form via outward-in fractional crystallization from a melt [4], outward-in crystallization due to significant volatilization at the surface of the melt droplet [5, 6, 7], or vapor-solid deposition of melilite on a preexisting core [8, 9].

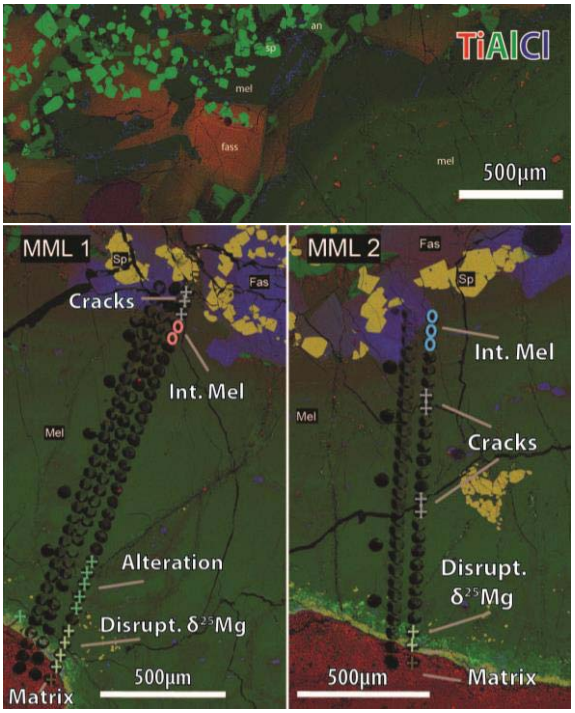

Figure 1. *Top:* TiAlCl (RGB) map showing distinctive oscillatory zoning, boundary between the core and mantle and interior phases. *Bottom:* Spot location for melilite mantle line 1 (MML1) and melilite mantle line 2 (MML2) shown on a MgAlTi (RGB) map, where Mg is Red, Al is Green, Ti is blue. Dark spots are laser ablation pits with a diameter of 50µm. For both locations, the line scan on the right is isotope data used in this study. The symbols correlate to their respective isochron (Fig. 2,3).

A more in-depth look at the petrography as well as stable Mg isotopes is presented in [10] and a major and trace element study is shown in [11]. Here we report a high-precision Al-Mg data set using an *in-situ* laser ablation MC-ICP-MS technique across two transects of the melilite mantle.

Methodology: EK 459-5-1 was characterized using a JEOL JSM-7600F SEM and a Cameca SX-100 electron microprobe at JSC. *In-Situ* Al-Mg isotope studies were done on a Nu Plasma II MC-ICP-MS with an Analyte 193nm excimer laser system. The laser was operated with a spot size of 50 µm, 10 Hz rep rate and a fluence of 2.99 J/cm^2. ^{24}Mg, ^{25}Mg, ^{26}Mg, and ^{27}Al were all measured simultaneously using the faraday cups of the multicollector. A natural gehlenite standard was used to correct for mass bias and instrument fractionation. $^{27}Al/^{24}Mg$ values were compared to electron microprobe data to verify the accuracy. The data are reported in δ notation relative to DSM3 [12]. A β value of 0.514 was used for calculating the radiogenic component of each data point ($\delta^{26}Mg^*$) [13].

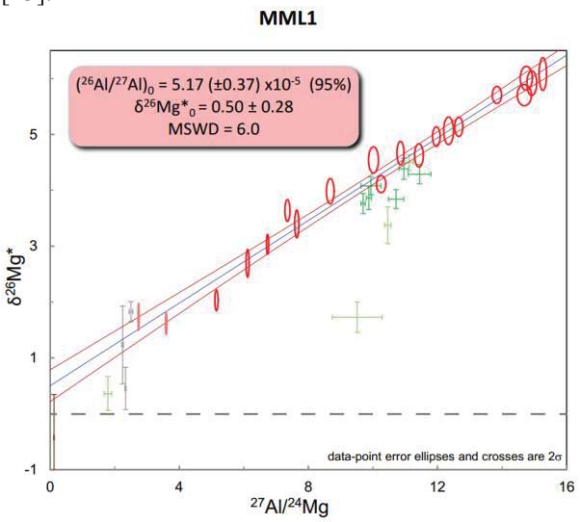

Figure 2. Al-Mg isochron for MML1. Regression yields a slope of 0.370 ± 0.027 (2σ.) on the plot of $\delta^{26}Mg^*$ vs. $^{27}Al/^{24}Mg$, which corresponds to a $(^{26}Al/^{27}Al)_0$ value of 5.17 (±0.37) x 10^{-5} (2σ). The isochron is produced using the melilite mantle line scan plus 2 interior melilite. Visibly altered spots, rim-ward spots showing disrupted $\delta^{25}Mg$

values and cracks, were not included in the regression and are shown as error crosses (see text). Model 1 of Isoplot (v. 4.13) was used

Results: Figure 1 (*bottom*) shows the 50µm (diameter) ablation pits for MML1 and MML2 (melilite mantle line scan 1,2). The right column of ablation pits are the isotope measurements presented in this study (Fig. 1). They are marked and color coded with their respective isochron diagrams (Fig. 2,3). The crosses are left out for each regression for the labeled reason but are displayed on the isochrons. The points labeled 'Disrupt. δ^{25}Mg' are the most rim-ward data points that show a sharp drop in δ^{25}Mg as discussed in [10], they also show a significant loss of ^{26}Mg* and are left out of the slope calculations. Ellipses are the valid data points used in the regressions. MML2 shows a well correlated regression (MSWD = 1.4) corresponding to a $(^{26}Al/^{27}Al)_0$ value of 5.92 (±0.16) x 10^{-5} (2σ) and a $\delta^{26}Mg^*_0$ value of 0.090 ± 0.098 (2σ). MML1 shows more scatter about the isochron (MSWD = 6.0), corresponding to a $(^{26}Al/^{27}Al)_0$ value of 5.17 (±0.37) x 10^{-5} (2σ) and a $\delta^{26}Mg^*_0$ value of 0.50 ± 0.28 (2σ). The anorthite in the core is visibly altered, and produce a $(^{26}Al/^{27}Al)_0$ value of ~4 x 10^{-5} (2σ) when tied to the low Al/Mg phases, with an MSWD >20.

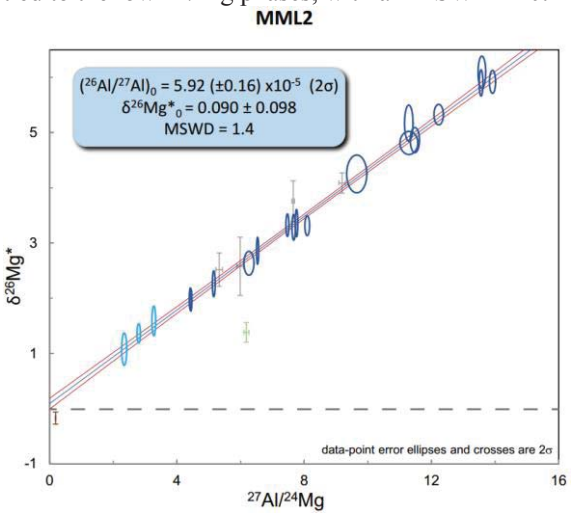

Figure 3. Al-Mg isochron for MML2. Regression produced a slope of 0.424 ± 0.011 (2σ) on the plot of δ^{26}Mg* vs. $^{27}Al/^{24}Mg$ corresponding to a $(^{26}Al/^{27}Al)_0$ value of 5.92 (±0.16) x 10^{-5} (2σ). The isochron was produced using melilite from the mantle as well as 3 interior melilite spots just past the core-mantle boundary. Similarly, spots placed on obvious cracks as well as the rim-ward disrupted δ^{25}Mg, were disregarded and shown as error crosses corresponding to Fig. 1. Isoplot model 1 was used to calculate the regression.

Discussion The resolvable, positive intercept of MML1 (Fig. 2) is likely evidence of closed system resetting as explored in [14]. MML2 is certainly a better fit regression compared to MML1. The slope of MML2 more correctly estimates the initial $^{26}Al/^{27}Al$ at the time of formation of the melilite mantle. The MML1 value is almost certainly a derivative of MML2. The oscillatory zoning of the mantle is likely related to the early formation event(s) of the mantle [8, 9]. This texture has also been reported in CAIs USNM 5241 [15, 4, 8, 9], and EGG-6 [8]. These CAIs are very similar to EK 459-5-1 both petrographically and chemically. The zoning is much less pronounced in MML1 and is also missing the small fassaite grains which line up with the chemical oscillations around almost the entire rest of the mantle (ex: Fig. 1, *top*). This seems to imply that this area has undergone a discrete thermal event which locally homogenized the chemical profile. This section is bound by two cracks which go hand in hand with areas of alteration. These cracks could have acted as conduits to essentially 'cook' this area, allowing for chemical and isotopic redistribution. This could be reasoning for the disturbed isochron of MML1, while not affecting MML2.

Under the likely assumption that the Solar System initial radiogenic Mg ($\delta^{26}Mg^*_0$) cannot be above 0 (relative to a terrestrial standard), we can better estimate the true initial $^{26}Al/^{27}Al$ of the object by producing a model isochron. When anchoring MML2 to the origin, the $(^{26}Al/^{27}Al)_0$ becomes more precise at 6.04 (±0.07) x 10^{-5} (2σ) with an MSWD = 1.5, this drops to 1.3 without changing $(^{26}Al/^{27}Al)_0$ when the three 'interior' melilite data points (light blue) are excluded. These three points are slightly enriched in ^{26}Mg* and are the reason for the almost positive $\delta^{26}Mg^*_0$ value of 0.090 ± 0.098 (2σ)

Even though EK 459-5-1 has undergone extensive reprocessing and is far from a pristine, nebular condensate, MML2 is still a well-constrained internal isochron of a resolvable, supra-canonical value. If homogeneous distribution of $^{26}Al/^{27}Al$ is assumed, then this study suggests the true $(^{26}Al/^{27}Al)_0$ of the Solar System is likely ≥ 6 x 10^{-5}, consistent with the studies of [16, 17, 14].

References: [1] Bouvier A. and Wadhwa M. (2010) *Nature Geosci, 3,* 637-641. [2] Wark D. A. and Lovering J. F. (1982) *GCA, 46,* 2581-2594. [3] Rubin A. E. (2012) *MAPS, 47, Nr 6*, 1062-1074. [4] MacPherson G. J. et al. (1989) *GCA*, 53, 2413-2427. [5] Kurat G. et al. (1975) *EPSL, 26*, 140-144. [6] Richter F. M. et al. (2006) *MAPS, 41,* 83-93. [7] Mendybaev R. A. (2006) *GCA, 70,* 2622-2642. [8] Meeker G. P. (1995) *MAPS, 30,* 71-84. [9] Meeker G. P. (1995) *LPS XXVI,* 947-948. [10] Kerekgyarto A. G. et al. (2014) *LPS XLV*, 2874. [11] Jeffcoat C. R. et al. (2014) *LPS XLV*, 2523. [12] Galy A. et al. (2003) *JAAS, 18*, 1352-1356. [13]Davis A. M. et al. (1990) *Nature, 347*, 655-658. [14] Simon J. I. and Young E. D. (2011) *EPSL*, *304*, 468-482. [15] El Goresy A. et al. (1985) *GCA, 47,* 1635-1650. [16] Young E. D. et al. (2005) *Science*, *308*, 223-227. [17] Simon J. I. et al. (2005) *EPSL, 238*, 272-283.